Numerical simulations of ceramic firing in catenary kilns

J. A. da Silva[1]*, G. G. Nery[1], L. C. Gómez[2], F. N. Teixeira[1], L. G. M. Guimarães[1]
[1]Federal University of São João del Rei, Departamento de Ciências Térmicas e dos Fluidos, 36307-352, Pç. Frei Orlando 170, São João Del Rei, MG, Brazil
[2]University of São Paulo, São Carlos School of Engineering, Heat Transfer Research Group, São Carlos, SP, Brazil

Abstract

Kiln geometries were developed to reach homogeneous temperatures above 900 °C, during the firing process, aiming to improve the production process of the ceramists from Vale do Jequitinhonha (MG/Brazil). Techniques of reactive flow numerical solution using the software Ansys CFX have been used to foresee the behavior of the firings. Two types of catenary geometries, simple and robust, were studied, capable of being easily reproduced. The firewood used as an energy source in the current kilns and the developed ones, in this research project, favored the control of the kiln's atmosphere during the firing, beyond being a source found with easiness for the ceramists. The results of the numerical simulations demonstrated the energy efficiency of the kilns and the level of temperature reached. Knowing well thermal and gas dynamic behavior, some parameters of the burning could be improved, aiming for a better quality of used ceramics.
Keywords: computer simulations, thermal analysis, energy efficiency, ceramic firing.

INTRODUCTION

The present work led with the numerical simulation of craft kilns used for ceramics production in the Jequitinhonha Valley, Minas Gerais, Brazil. Work with clay in Jequitinhonha Valley began with the manufacture of utilitarian pieces that were made by women called pan makers. The tradition was maintained through the generations: grandparents, mothers, and daughters. They fabricated jugs, pots, pans, and jars, all with a marked influence on native Indians. They also produced figures to adorn cribs and toys used by children. In the course of time, they began to produce decorative pieces, human figures, animals, everyday scenes, types, uses, and customs of the region. Currently, these pieces produced in the valley have great demand and value in the 'internal' market. However, due to the rudimentary production process, the pieces do not have good mechanical resistance and end up breaking during transportation. The reason for this weakness is mainly due to the formation of a black heart, which happens due to the quick raising of the furnace temperature, sealing and burning the clay outside, leaving the inside poorly sintered and with impregnated carbon inside. The carbon coming from the organic matter (responsible for gray clay) usually must be removed by burning in the form of carbon dioxide, which escapes through the pores of the clay, when the firing procedure is done slowly. An improvement to the burning process is required to minimize these effects, besides the search for higher energy efficiency of the process ensuring productivity and market competitiveness. In this paper, we sought to understand the firing process and operating procedures that influence the temperature distribution and firewood consumption in the kiln. For this purpose, catenary kiln simulations were performed using the software Ansys CFX. In recent years, the bibliography presents a few works that address the issue of burning in catenary furnaces and the prediction of burning parameters through simulations [1-5]. Studies on issues related to burning parameters and even numerical simulations for combustion and radiation models were carried out [6-12].

Previous studies have shown the importance and convenience of the application of numerical simulations for the evaluation and analysis of firing procedures [13, 14]. The literature regarding ceramic firing in craft kilns is very limited due to the empirical characteristic of the development of this technology. When it is related to catenary kilns, it is even more difficult to find information in the literature [13, 15]. It is possible to find some studies about the application of numerical modeling to industrial kilns that operate with temperatures around 1000 °C. Possamai et al. [16] presented a study using numerical modeling on a ceramic frit production kiln. Nieckele et al. [17] applied numerical modeling on an aluminum melting furnace. Both research groups demonstrated the complexity to work with high-temperature kilns when using turbulence, combustion, and radiation models. Hachem et al. [18] and Abassi and Khoshmanesh [19] carried out studies with similar techniques, revealing the heat flux distributions and the presence of hot spots inside the kiln. For the understanding of the firing process and combustion phenomena, studies regarding tunnel kilns used in the structural ceramic industry can help with the mathematical modeling and determination of boundary conditions. Dugwell and Oakley [20] studied the heat transfer process in tunnel kilns, measuring the heat transfer between air and sides, top and back of the column, where they represented the whole column of bricks with a

**jant@ufsj.edu.br*
https://orcid.org/0000-0003-4813-1029

solid chrome magnesite block. Karaush et al. [21] performed an experimental study regarding the heat absorption from the radiating walls of a kiln by the ceramic ware set up in a kiln car, finding that there is an optimal spacing between the pieces which any further increase would not increase the heat absorption by the ceramic ware. Oba et al. [22] presented a thermal analysis of a tunnel kiln used for the production of roof tiles, fueled by firewood and shale oil, using a tridimensional numerical model based on the finite volume method to model the thermal behavior of the kiln. Nicolau and Dadam [14] performed a numerical and experimental analysis of a tunnel kiln used to fire ceramic bricks, stating that a correct simulation strategy allows the verification of the influence of a single variable in the kiln behavior while maintaining the others constant. It is also possible to perform a theoretical analysis of a determined set of parameters, without interfering with the kiln operation. Naccache et al. [23] investigated the flow and heat transfer of combustion gases in a tunnel kiln, using a bi-dimensional simplified approach, solving governing conservation equations by the finite volume method and using Fluent software with a non-uniform structured mesh. Santos [24] studied a kiln fueled with sawdust used to fire bricks, adapting it to be fueled with natural gas, doing his evaluations with a numerical algorithm developed to reproduce the thermal behavior, detailing the heat flow and energy consumption of the kiln. In the same year, Essenhigh [25] presented an analysis of a tunnel kiln, exploring its energy integral equation to evaluate the relation between energy input and useful output energy. Song [26] presented a study with three ceramic sintering tunnel kilns, showing the temperature curves and analyzing the temperature and atmosphere air distribution in the tunnel. A numerical simulation is a powerful tool, allied to its low cost it helps to understand the processes and even helps with the engineering of more adequate designs for the equipment. Carvalho and Nogueira [27] demonstrated the numerical analysis of the kiln firing process as a tool to improve the optimization of the kiln design. Zhao et al. [28] evaluated convection and radiation heat transfer inside an externally-fired kiln, representing a model for a drying or annealing furnace, applying a Monte Carlo method for calculating the radiation, and a control volume formulation for the convection heat transfer, in a 2D model of the 2x0.75 m kiln. Durakovic and Delalic [29] developed a mathematical model to analyze and check a stationary temperature field in the products and inside the kiln. Mancuhan et al. [30] developed a one-dimensional model, considering the gas flow, heat transfer, and evaporation of bound water in the preheating zone of a tunnel kiln, discovering that when no ambient air is fed, the gas temperature increases, affecting the product quality. Refaey et al. [31, 32] studied the application of guide vanes in the cooling zone of a tunnel kiln to reduce energy consumption in brick manufacturing, showing that the use of guide vanes increases heat transfer rates with all settings.

This article, analyze how the firing occurs in two types of catenary furnaces with different geometry, comparing the measured experimental data, in the built prototypes, with values obtained in computer simulations. It was possible to predict the behavior in its interior of the temperatures, fraction of unburned fuel, and degree of turbulence in an oxidizing and reducing atmosphere. We understand that the work can help with important information in the control of firing for artisanal potters in the Jequitinhonha Valley region of Minas Gerais, substantially improving the quality of artistic ceramics produced in the region. This paper aims to present two distinct geometries of catenary kilns for firing artistic ceramics, which seek to achieve better levels of firing temperature, as well as understanding important firing parameters, demonstrating by numerical simulations the possibilities of improvements.

METHODOLOGY

The simulations were performed aiming at the solution of conservative equations, in order to obtain the temperature field, streamlines, and fuel mass fractions. Due to the difficulty to perform a simulation regarding the firewood combustion, the fuel considered for the process was butane (C_4H_{10}), which was available in the software library. Another limitation of the software made it necessary to perform the simulation in the steady flow condition. The boundary conditions were determined based on the results from the experimental study, such as the firewood consumption, necessary to calculate the equivalent butane fuel flow. Another essential boundary condition was the pressure differential generated between the chimney exit and the air intakes, which must be lower in the chimney exit to represent the correct flow inside the kiln. The fluid model chosen was 'thermal energy', which considers and models the enthalpy transportation model through the defined domain, being more adequate to low-speed flows where the kinetic energy effects are negligible. The turbulence model applied was the standard k-ε model [33-35], due to its reliability. In this model, two variables are inserted into the equation system, one regarding turbulent kinetic energy, k, in m^2/s^2, and another for turbulence eddy dissipation, ε, in m^2/s^3. For the radiation model, the P1 model was chosen due to its characteristics of adding a transport equation for the simulation, being adequate for the pulverized fuel flames study [33]. The domain surfaces were considered opaque and diffuse, and the inlets and outlets of the furnace were transparent regions. The Gray model was applied to the 'spectral model', which assumes that all radiation is uniform throughout the whole spectrum [33]. Follow the main solved balance equations.

Balance equations: the system of equations solved in the Ansys CFX V11 software was composed of the following conservative equations. Continuity equation:

$$\frac{\partial \rho}{\partial t} + \nabla.(\rho \mathbf{V}) = 0 \qquad (A)$$

where ϱ and **V** stand for the transient local fluid density and velocity vector, respectively. These variables are mean temporal averaged values regarding the small time scales

of the Reynolds averaging procedure. Linear momentum conservation equation:

$$\frac{\partial(\rho\mathbf{V})}{\partial t}+\nabla.(\rho\mathbf{V}\otimes\mathbf{V})=-\frac{\partial p'}{\partial x}+\vec{\nabla}\cdot\{\mu_{eff}[\vec{\nabla}\mathbf{V}+(\vec{\nabla}\mathbf{V})^{T}]\}+\rho\mathbf{B} \quad (B)$$

where B is the sum of body forces, μ_{eff} is the effective viscosity accounting for turbulence, and p' is the modified pressure. μ_{eff} and p' are given respectively by:

$$\mu_{eff}=\mu+\mu_t \quad (C)$$

$$p'=p+\frac{2}{3}\rho k \quad (D)$$

where μ and μ_t represent the molecular and turbulent viscosity, respectively, and p is the transient local fluid pressure. The k-ε model uses the eddy viscosity concept, assuming that the turbulence viscosity is computed by:

$$\mu_t=c_\mu\rho\frac{k^2}{\epsilon} \quad (E)$$

where C_μ is a model constant. The quantities k and ε are computed directly from the resolution of the following differential transport equations:

$$\frac{\partial(\rho k)}{\partial t}+\nabla.(\rho Vk)=\vec{\nabla}.\left[\left(\mu+\frac{\mu_t}{\sigma_k}\right)\vec{\nabla}k\right]+P_k-\rho\varepsilon \quad (F)$$

$$\frac{\partial(\rho\epsilon)}{\partial t}+\nabla.(\rho V\varepsilon)=\vec{\nabla}.\left[\left(\mu+\frac{\mu_t}{\sigma_k}\right)\vec{\nabla}\epsilon\right]+\frac{\epsilon}{k}(C_{\varepsilon1}Pk-C_{\varepsilon2}\rho\varepsilon) \quad (G)$$

being $C_{\varepsilon1}$, $C_{\varepsilon2}$, σ_k, and σ_e model constants and P_k representing the turbulence production tensor due to viscous forces. The buoyancy forces are not considered in the present work. This last term is modeled as:

$$\mathbf{P}_k=\mu_t\vec{\nabla}\mathbf{V}.[\vec{\nabla}\mathbf{V}+(\vec{\nabla}\mathbf{V})^{T}]-\frac{2}{3}(\vec{\nabla}.\mathbf{V})(3\mu_t\vec{\nabla}.\mathbf{V}+\rho k) \quad (H)$$

If the flow is incompressible the mean velocity divergence is zero. In this case the second term of Eq. H does not contribute to turbulence production. In the present simulations, the flow is also considered compressible. In these cases, all the above terms are taken into account. The standard k-ε model employs values for the constants that were found by comprehensive data fitting for a wide range of turbulent flows. The values of these constants were C_μ=0.09, $C_{\varepsilon1}$=1.44, $C_{\varepsilon2}$=1.92, σ_k=1.00 and σ_e=1.30. The energy conservation equation was formulated in terms of the total energy ($e+V^2/2$) by the following equation:

$$\rho\frac{D}{Dt}\left(e+\frac{V^2}{2}\right)=\rho\dot{q}+\frac{\partial}{\partial x}\left(k_{eff}\frac{\partial T}{\partial x}\right)+\frac{\partial}{\partial y}\left(k_{eff}\frac{\partial T}{\partial y}\right)+\frac{\partial}{\partial z}\left(k_{eff}\frac{\partial T}{\partial z}\right)-\frac{\partial(up)}{\partial x}-\frac{\partial(vp)}{\partial y}-\frac{\partial(wp)}{\partial z}+\frac{\partial(u\tau_{xx})}{\partial x}+\frac{\partial(u\tau_{yx})}{\partial y}+\frac{\partial(u\tau_{zx})}{\partial z}+\frac{\partial(v\tau_{xy})}{\partial x}+\frac{\partial(v\tau_{yy})}{\partial y}+\frac{\partial(v\tau_{zy})}{\partial z}+\frac{\partial(w\tau_{xz})}{\partial x}+\frac{\partial(w\tau_{yz})}{\partial y}+\frac{\partial(w\tau_{zz})}{\partial z}+\bar{\Phi}+\rho.\mathbf{f}.\mathbf{V} \quad (I)$$

where $\bar{\Phi}$ stands for the turbulent viscous dissipation contribution and k_{eff} is the effective thermal conductivity calculated by $k_{eff}=k+\mu t.C_p/Pr_t$, being Pr_t the turbulent Prandtl number and C_p the specific heat at constant pressure. Transport equations: the transport equations for the chemical species that appear and disappear in the chemical reaction were modeled in CFX V11 combustion models with the same algorithms used for multicomponent flows, with the addition of a source term due to the chemical reaction. The transport equation for the component I with mass fraction Y_I is:

$$\frac{\partial(\rho Y_I)}{\partial t}+\vec{\nabla}.(\rho\mathbf{V}Y_I)=\vec{\nabla}.(r_{Ieff}\vec{\nabla}Y_I)+S_I \quad (J)$$

where S_I is the source term due to the rate of a chemical reaction involving component I. The main modeled components were oxygen, hydrogen, nitrogen, water, and butane. Rate of chemical reaction: in general, chemical reactions can be described in terms of K elementary reactions involving N_c components which can be written as:

$$\sum_{I=A,B,C,...}^{Nc}v'_{kI}I\leftrightarrow\sum_{I=A,B,C,...}^{Nc}v''_{kI}I \quad (K)$$

where v_{kI} is the stoichiometric coefficient for a component I in the elementary k reaction. The rate of production/consumption, S_I, of component I may be computed by summing the rate of progression of every elementary reaction that component I participates as:

$$S_I=W_I\sum_{k=1}^{K}(v''_{kI}-v'_{kI})R_k \quad (L)$$

where R_k is the elementary reaction rate for the k reaction. In CFX this term can be calculated, using the model of viscous dissipation.

Boundary conditions: in Fig. 1 the simulated geometries and a photograph of the experimental furnace are shown. The geometries were developed following the guidelines presented by Gregory [36] and Olsen [37]. The furnace in Fig. 1a had a useful volume capable of meeting the production of various artisans, and the furnace in Fig. 1b had a small useful volume serving for household production. They were called community kiln and family kiln, respectively. In Fig. 1c the furnace with a small volume of 0.2 m^3 employed for ceramists from Jequitinhonha Valley is shown. Two sets of inlet and outlet boundary conditions were considered for the simulation of each kiln. The community kiln simulations were named A1 and A2, and the family kiln B3 and B4, as shown in Table I. In the simulations, the influences of the damper positioning and air intakes were analyzed, in order to ascertain the impact on the temperature variation and the mass fraction of oxygen and butane. The characteristics of the fuels used are shown in Table II. The assumed inlet and outlet sections of both kilns in the simulations are shown in Fig. 1.

As can be seen in Table I, the static pressure values were fixed at the inlet and outlet sections, while the inlet

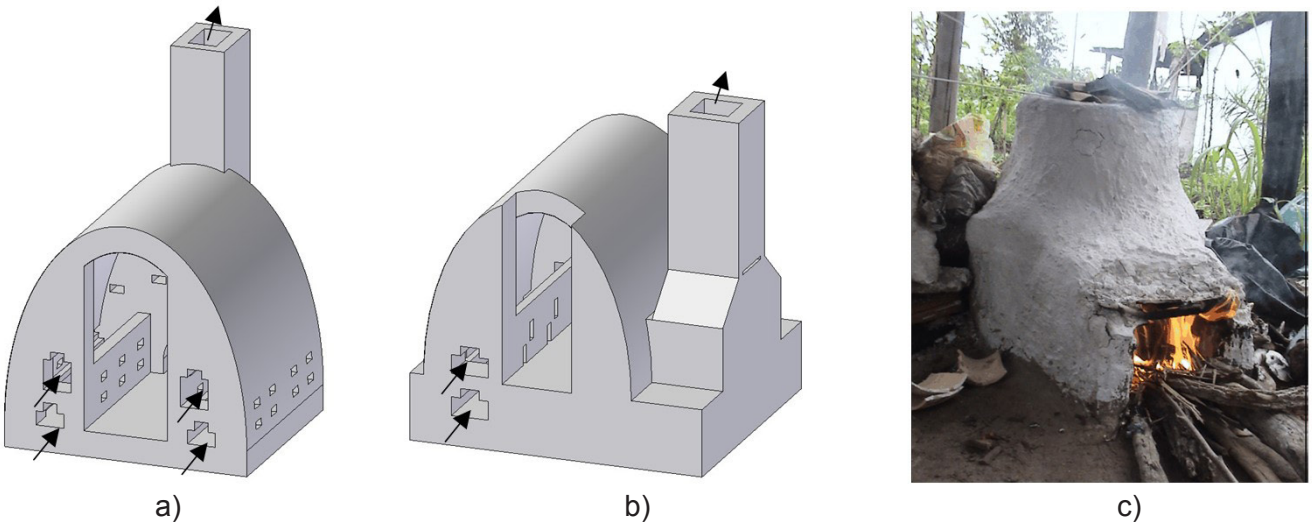

Figure 1: Schematics of the community kiln with 1.42 m^3 useful volume (a) and family kiln with 0.6 m^3 useful volume (b) and image of a rudimentary kiln used by potters of 0.2 m^3 (c).

Table I - Summary of the basic settings of each simulation.

Simulation	Damper opening (%)	Air inlet (%)	Air inlet pressure (Pa)	Outlet pressure (Pa)	Butane in (m/s)
A1	100	100	101325	101322	0.000826673
A2	50	50	101325	101324	0.000826673
B3	100	100	101325	101322	0.003827722
B4	50	50	101325	101324	0.003827722

Table II - Lower heating value (LHV) and specific volume value for butane and wood [38, 39].

Fuel	LHV (kcal/kg)	Specific volume (m^3/kg)
Butane	11800	0.4
Firewood	3000	0.002

butane velocity was fixed at the kiln inlet sections. The fuel consumption was calculated for simulations A1, A2, B3, and B4, using Eqs. M to O in order to determine the volumetric flow rate and velocity of butane that must be burned to provide the same amount of heat that would provide wood. The obtained values are presented in Table III. The butane mass flow rate was calculated by Eq. M using the known wood mass flow rate and both the butane and wood lower heating values (LHV). Now multiplying by the butane specific volume, the volumetric mass flow rate was obtained (Eq. N). Taking the area of the kiln as being 0.8372 m^2, it was defined the velocity of fuel input into the simulation (Eq. O).

$$\dot{m}_{Butane} = \frac{LHV_{Wood}.\dot{m}_{Wood}}{LHV_{butane}} \quad (M)$$

$$\dot{\forall}_{Butane} = \dot{m}_{Butane}.v_{Butane} \quad (N)$$

$$V_{Butane} = \frac{Flow_{Butane}}{Area} \quad (O)$$

Table III - Butane volumetric consumption per second and inlet velocity values in the kilns.

Rate	Family kiln	Community kiln
$\dot{\forall}_{Butame}$ (m^3/s)	0.0012994350	0.0006920903
V_{Butane} (m/s)	0.0038277220	0.0008266727

The computational kiln domain was generated with the available CAD (computer-aided design). The meshes were constructed in the obtained computational domains. The adjustment of size and shape of the mesh elements was made according to the first obtained simulations results, in order to optimize the results and allocation of computing resources. With the first results, it was noticed that the very small size of mesh elements would result in an excessive simulation time, with few changes in the thermal field distribution and gas flow. Table IV shows the mesh sizes employed in the simulations A1, A2, B3, and B4.

Table IV - Employed mesh sizes in the kiln simulations.

Simulation	Nodes	Elements
A1	20109	100860
A2	20103	100559
B3	29099	151855
B4	29120	151606

EXPERIMENTAL RESULTS

Both family and community kilns were built in the Federal University of São João Del Rei (UFSJ) following the Olsen principles [8, 9, 20, 21, 23, 36], as shown in Fig. 2. During the firing procedure, the temperature levels were obtained by several thermocouples placed inside the kilns. For the correct instrumentation of the community kiln, eight thermocouples were placed along the left side of the chamber to collect the temperature over the furnace with more precision. The thermocouples disposal is shown in Fig. 3.

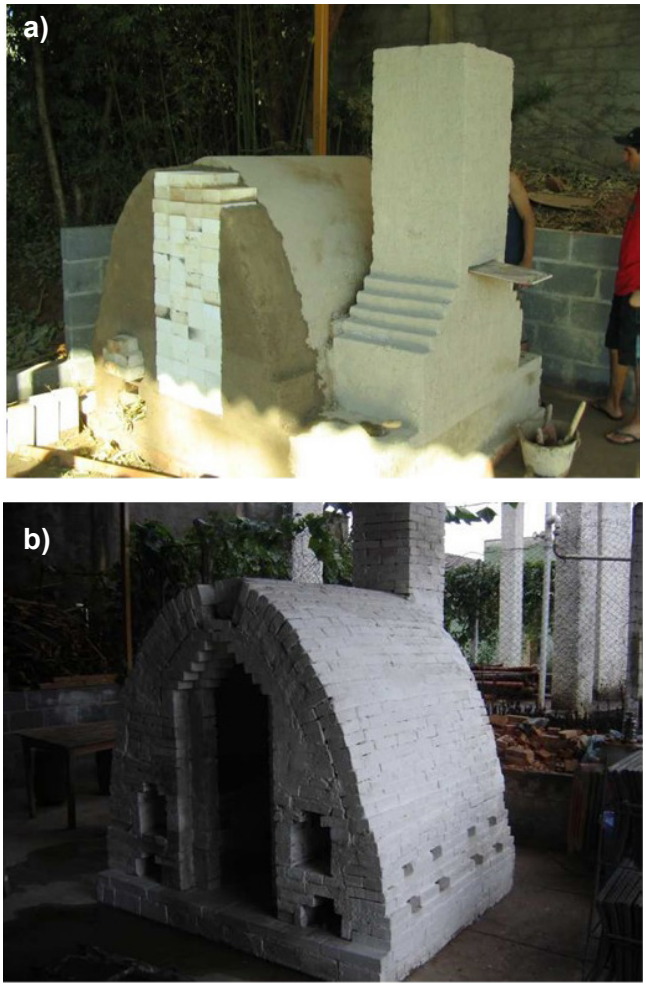

Figure 2: Images of the family kiln (a) and community kiln (b) built at UFSJ.

The firewood used in the firing procedure was weighed and characterized to calculate the energetic consumption. The firing was performed following an adapted heating curve used by the Jequitinhonha Valley potters. In Fig. 4a the temperature levels measured by the thermocouples during the firing in the community kiln are shown. As can be noted, almost all temperatures were equal, except those measured with thermocouples T3 and T8. These temperature values were smaller because these thermocouples were installed at the entrance and bottom of the kiln. For the instrumentation

Thermocouples disposal in the community kiln

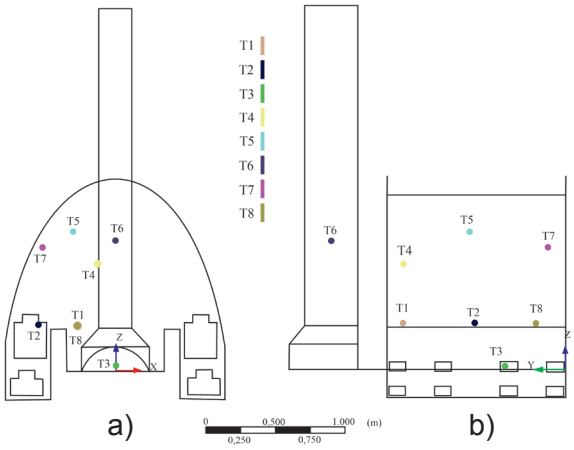

Figure 3: Schematics showing the thermocouples disposal in the community kiln: a) front view; and b) side view.

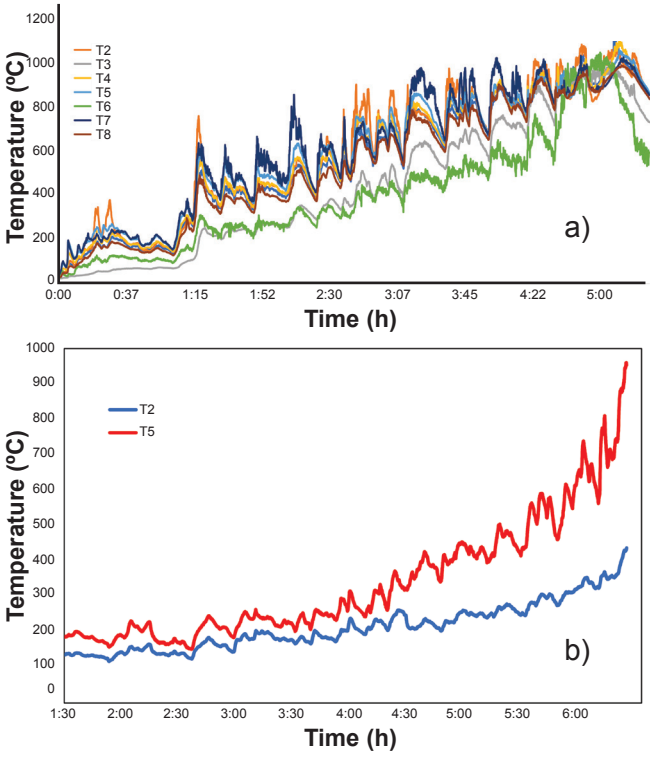

Figure 4: Temperatures measured by the thermocouples during the firing with: a) community kiln; and b) family kiln.`

of the family kiln, only two thermocouples were used, one in the central region of the kiln, and the other placed in the chimney. The firewood used in this kiln had the same conditions as the firewood used in the community kiln. In Fig. 4b the results obtained by the thermocouples during this procedure are shown. Both the family and community kiln thermocouples were verified by an experimental uncertainty analysis [40], showing an average level of error of 1.42% for all temperature values. It was estimated that this was an acceptable error for the analysis of the kilns' temperature levels and their variations.

NUMERICAL SIMULATION RESULTS

The simulations' results for the community kiln were obtained through simulations A1 and A2, while the results for the family kiln were obtained by simulations B3 and B4. Whenever possible, the simulation results were compared to address the influence of the damper opening degree. The results were also compared to the experimental ones, quantitatively. The simulation results were presented in central Cartesian planes displayed inside the computational domains, showing temperature, fuel, and oxygen mass fraction fields, as well as streamlines. In Fig. 5 simulated temperature fields in the plane situated in the middle section of the community kiln with the damper completely opened are presented (Fig. 5a, simulation A1) and partially opened at 50% (Fig. 5b, simulation A2). The kiln with the damper fully opened and operating with all air inlets reached a maximum temperature of 745 °C. Otherwise, when the partially opened damper was used (simulation A2), the same kiln reached maximum temperature levels of about 860 °C. This behavior could be an indication that the kiln with a partially closed damper employed better the chemical energy available in the fuel, producing combustion products with higher temperatures in the kilns. In this case, the hydraulic resistance at the chimney inlet seems to be beneficial. In fact, in simulation A2 the temperature distribution was more homogeneous (Fig. 5b). In this case, due to the partial closure of the damper and air inlets, a decrease in the cold air volume entering the furnace occurred. This was beneficial to reduce the temperature gradients inside the kiln and maintaining a higher level of temperature. In the region of the chimney situated above the damper, a recirculation of atmospheric air caused a significant cooling of the exhaust gases. The use of the partially closed damper prevented the cold air to influence more the bottom regions of the kiln. The bottom areas of the furnace and the chimney were the ones that showed the highest levels of temperature. This behavior was due to strong air circulation, which caused the entrainment of gas not yet burnt in the region of the chimney. Furthermore, the front wall of the kiln remained with low temperatures due to the intense airflow from the inlet of the furnace and the ashtray, predominantly an oxidizing atmosphere [14, 15]. The results displayed in Fig. 5b can be qualitatively compared with the measured temperatures displayed in Fig. 4a. It can be noted that the values of the simulated stationary temperature field were between 800 and 900 °C, in almost all kiln regions. These values were in agreement with the majority of measured temperatures, considering the values obtained after 3 h of kiln operation.

In Figs. 6a and 6b the fuel mass fraction values obtained for simulations A1 and A2, respectively, are displayed. As can be noted, the fuel mass fractions presented very low levels or close to zero, overall for the completely open damper (simulation A1). This could indicate that when the damper is completely open some quantity of the fuel is not burned and is expelled through the chimney. It was observed that with the partially open damper the fuel mass fraction

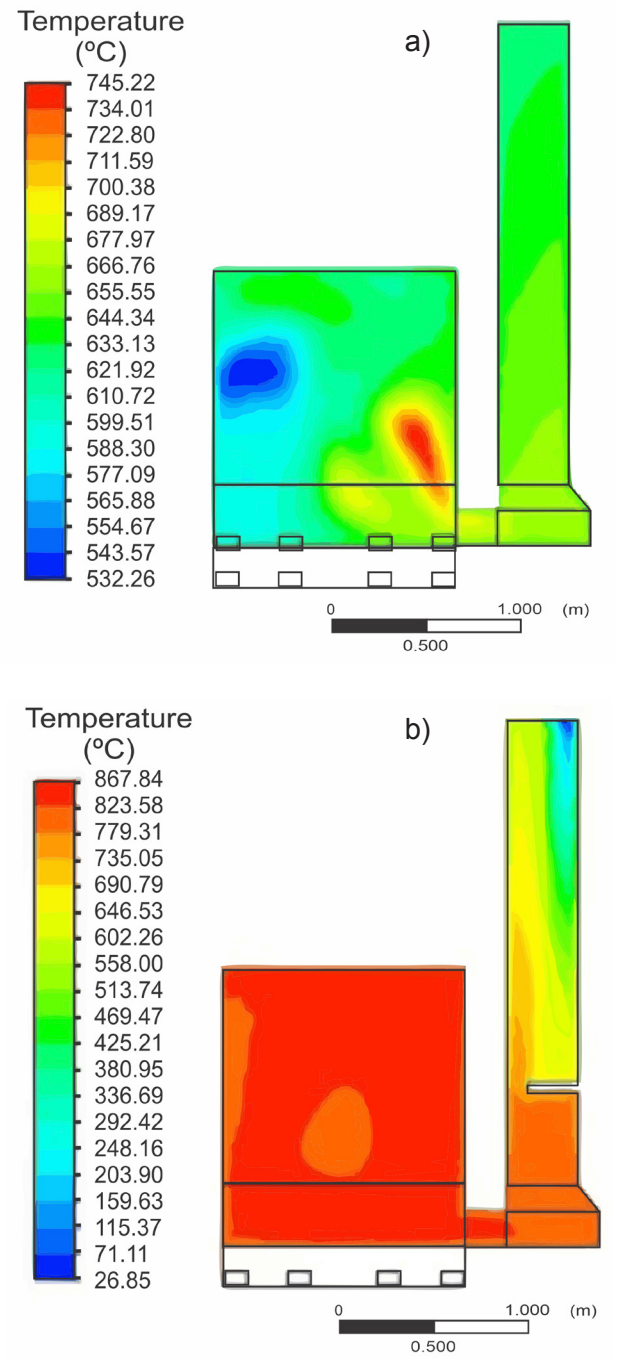

Figure 5: Temperatures displayed through the YZ plane and located at the central position for simulations A1, 100% open damper (a), and A2, 50% open damper (b), of the community kiln.

was slightly higher and more symmetrically distributed in the kiln. This could be the cause of better efficiency of the combustion process and higher kiln temperatures. The simulated oxygen mass fractions for simulations A1 and A2 are presented in Figs. 6c and 6d, respectively. It is interesting to note that the regions where the mass fractions of oxygen and butane approach zero are those of the highest temperatures (Fig. 5). Curiously, in these regions, the butane mass fractions were the highest (Figs. 6a and 6b). This fact indicated that in these regions the chemical reaction was

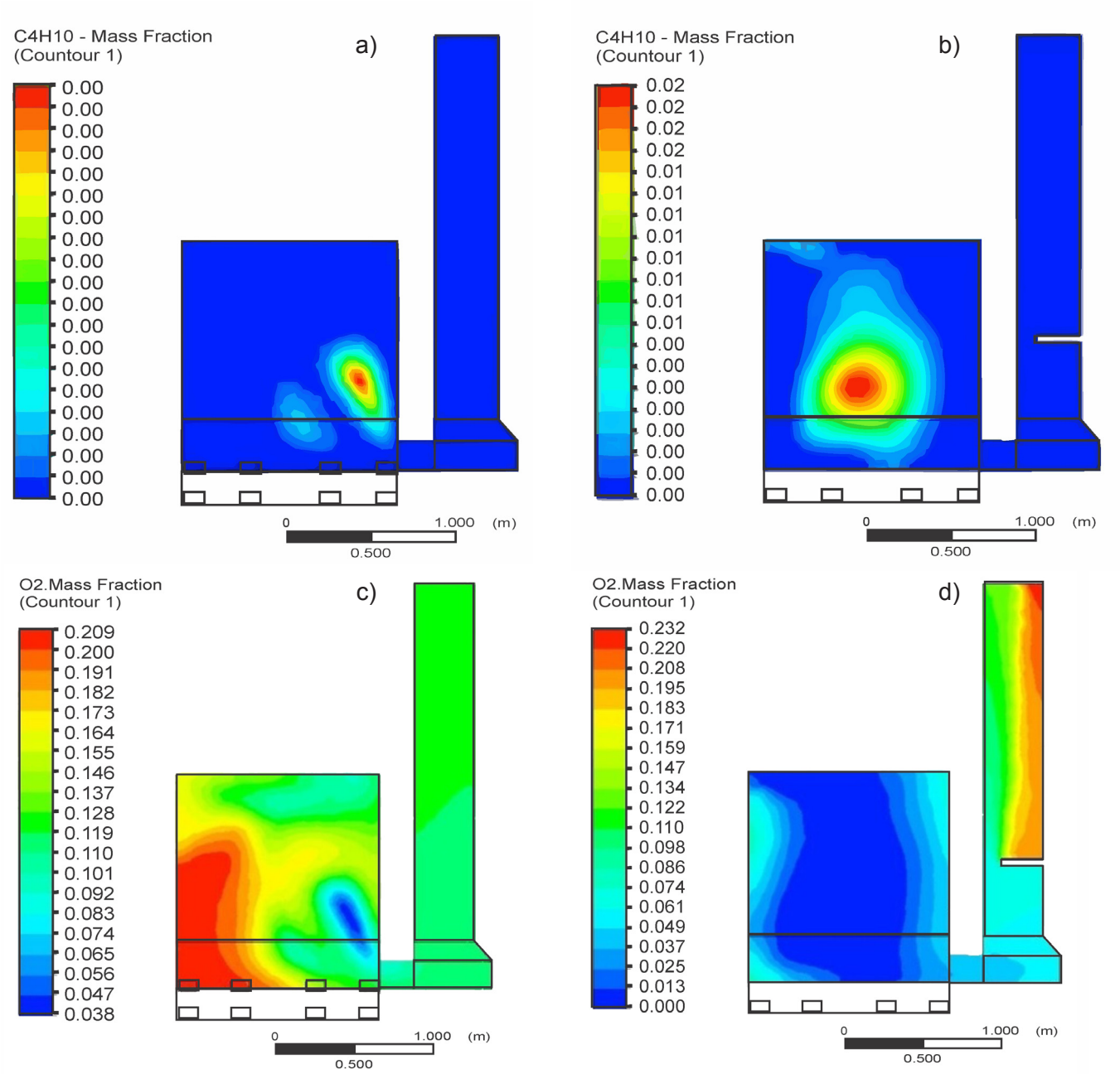

Figure 6: Mass fractions of fuel C_4H_{10} (a,b) and oxygen (c,d) displayed through the YZ plane and located at the central position for simulations A1, 100% open damper (a,c), and A2, 50% open damper (b,d) of the community kiln.

very close to the stoichiometric condition, being slightly rich. In fact, regions with an excess of air were the ones with lower temperatures. These results indicated that for optimum combustion efficiency, the kiln should operate in a condition near the complete burning of the fuel with no excess air [7-9]. Observing Fig. 6d, it can be proven with the increase of the mass fraction of oxygen in this region. The simulated turbulent flow velocities for both simulations are displayed in Fig. 7. The speed values obtained for the completely opened damper were higher than those obtained for the kiln with a partially opened damper. The circulation inside the kiln in the former case was more intense, leading to the lowest temperature values (Fig. 7a) and to a better flow through the kiln. In the second case, the partially opened damper imposed a restriction in the passage of the gases in the chimney, increasing the overall pressure drop, but resulting in a smaller pressure difference between the flue gas exit (right before the damper) and entry of air into the furnace. This behavior led to high temperatures inside the kiln (Fig. 7b) due to the smaller air speed and a more efficient combustion reaction.

The family kiln simulations (B3 and B4) also provided good results in relation to the experimental results. In this kiln, the temperature was measured in two places only, due to the smaller size of the furnace. In Fig. 8b the temperature values simulated with the partially open damper (simulation

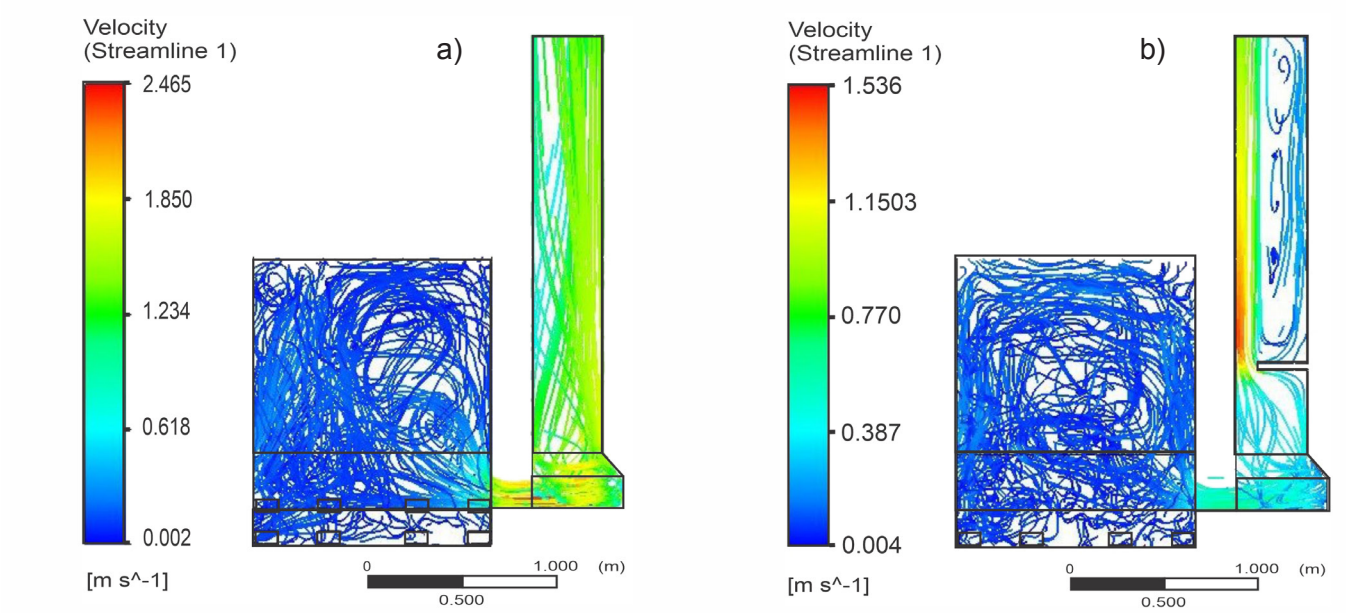

Figure 7: Current lines of velocity and turbulence occurring inside the domains studied in simulation A1, 100% open damper (a), and simulation A2, 50% open damper (b), of the community kiln.

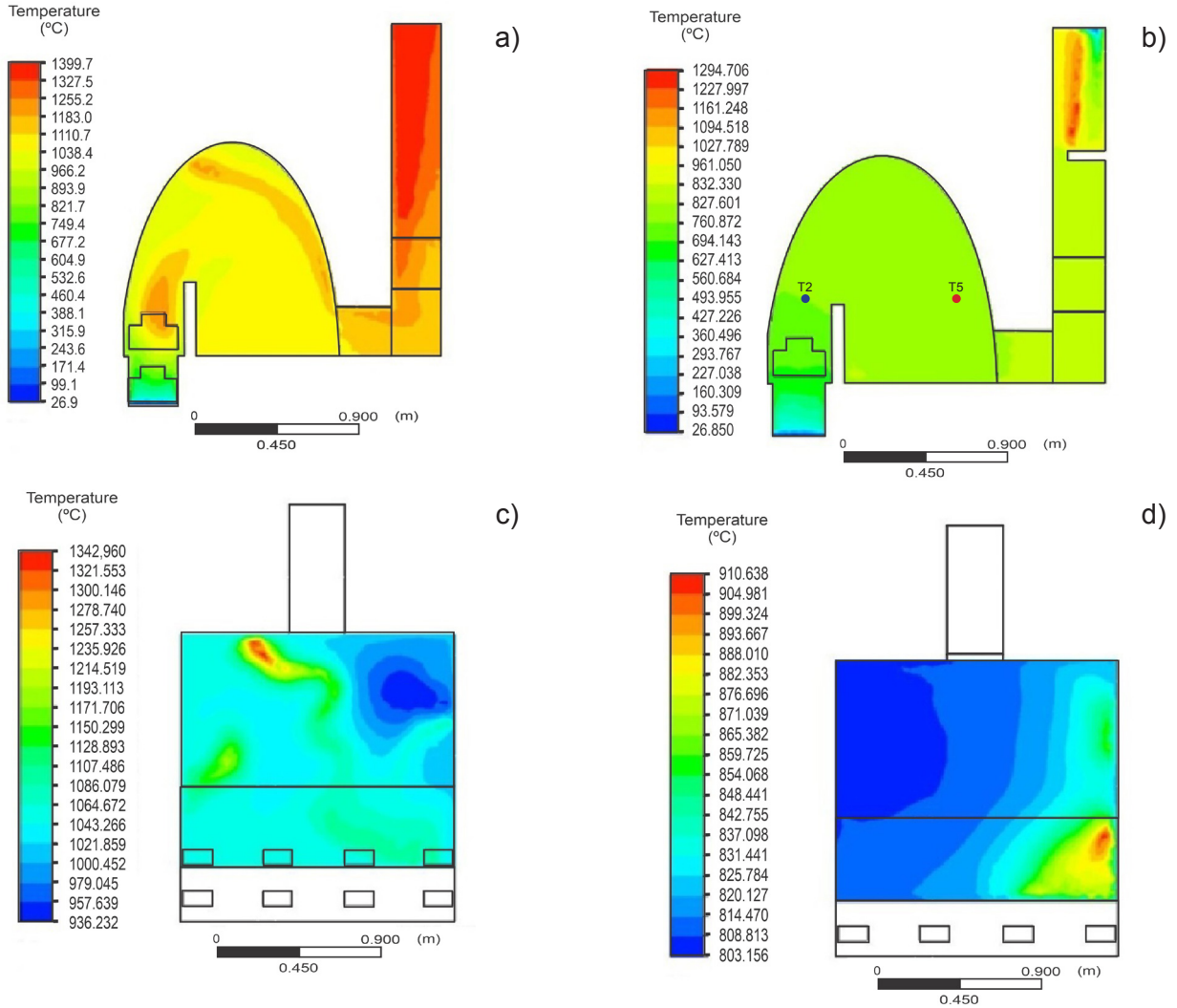

Figure 8: Temperatures displayed through the XZ plane for 100% open damper (a) and 50% open damper (b), and the YZ plane for 100% open damper (c) and 50% open damper (d) of the family kiln.

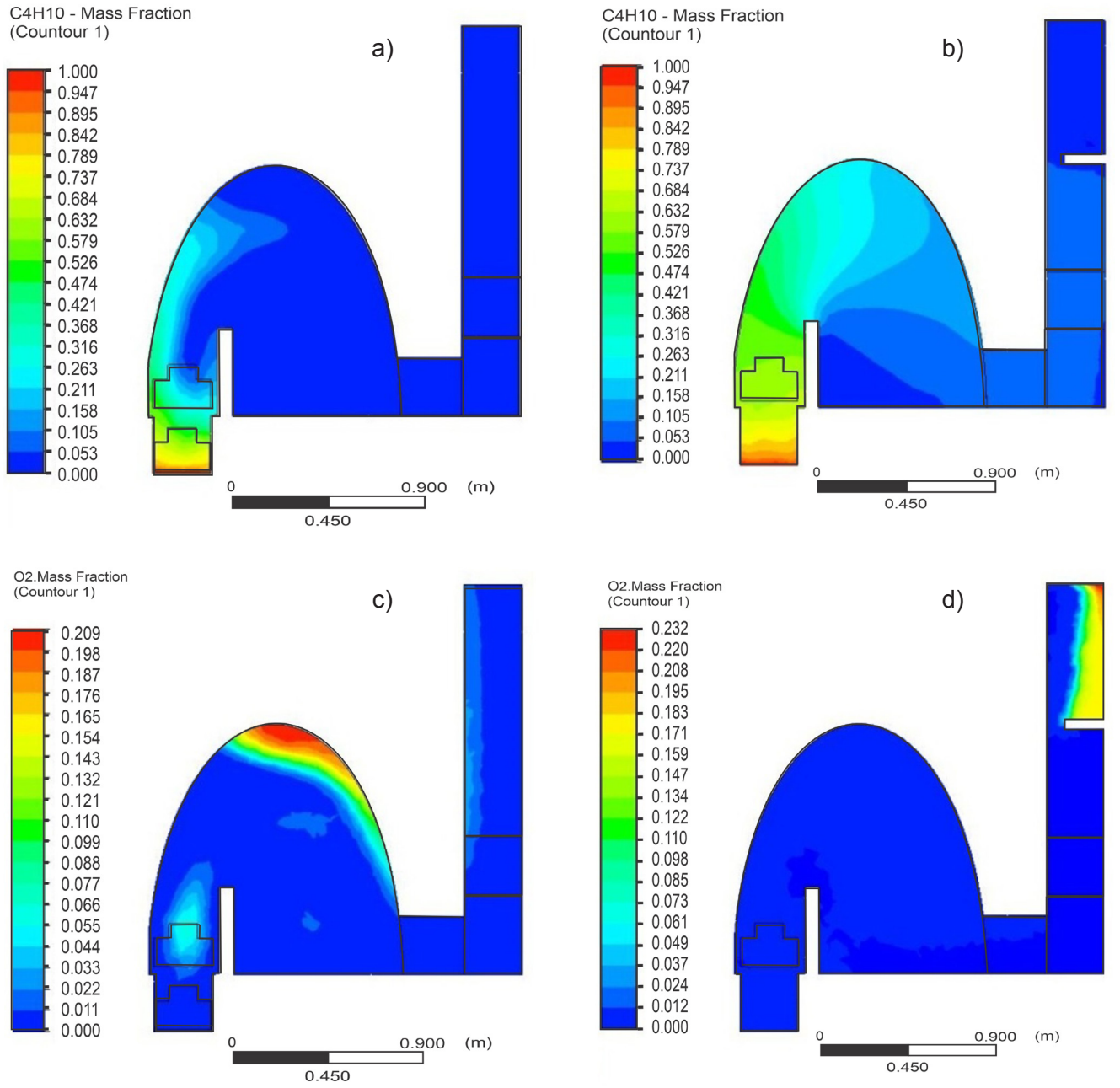

Figure 9: Mass fractions of fuel C_4H_{10} (a,b) and oxygen (c,d) displayed through the XZ plane and located at the center position of the furnace for simulations B3, 100% open damper (a,c), and B4, 50% open damper (b,d), of the family kiln.

B4) are presented, which can be compared with those experimentally measured for the family kiln (Fig. 4b). As can be noted, this kiln resulted in higher values of temperatures during the firing, considering both the simulation and the experimental results. The simulated temperature fields of the family kiln are presented in Fig. 8 for simulations B3 and B4, and two values of damper opening in two different planes. The higher temperature levels, reaching peaks of 1340 °C, were obtained within the kiln chamber in simulation B3 (totally open damper), as shown in Fig. 8c. For this same case, temperatures between 1300 and 1400 °C were obtained in the chimney (Fig. 8a). These results indicated that there was unburned fuel being removed to the atmosphere. This was due to intense circulation and a flow with higher velocity. This behavior resembled that observed in the experiment of the community kiln where the temperature levels in the chimney outperformed the other internal kiln regions at the end of the firing due to the intensity of the draft (Fig. 5a) [1, 6, 7].

In simulation B4, the temperature range varied between 800 and 900 °C according to Figs. 8b and 8d. As observed in the results of simulation A2, the closure of the damper caused a reduction in flow velocity and in the oxygenation of the furnace (Fig. 6d). For this reason, the temperature

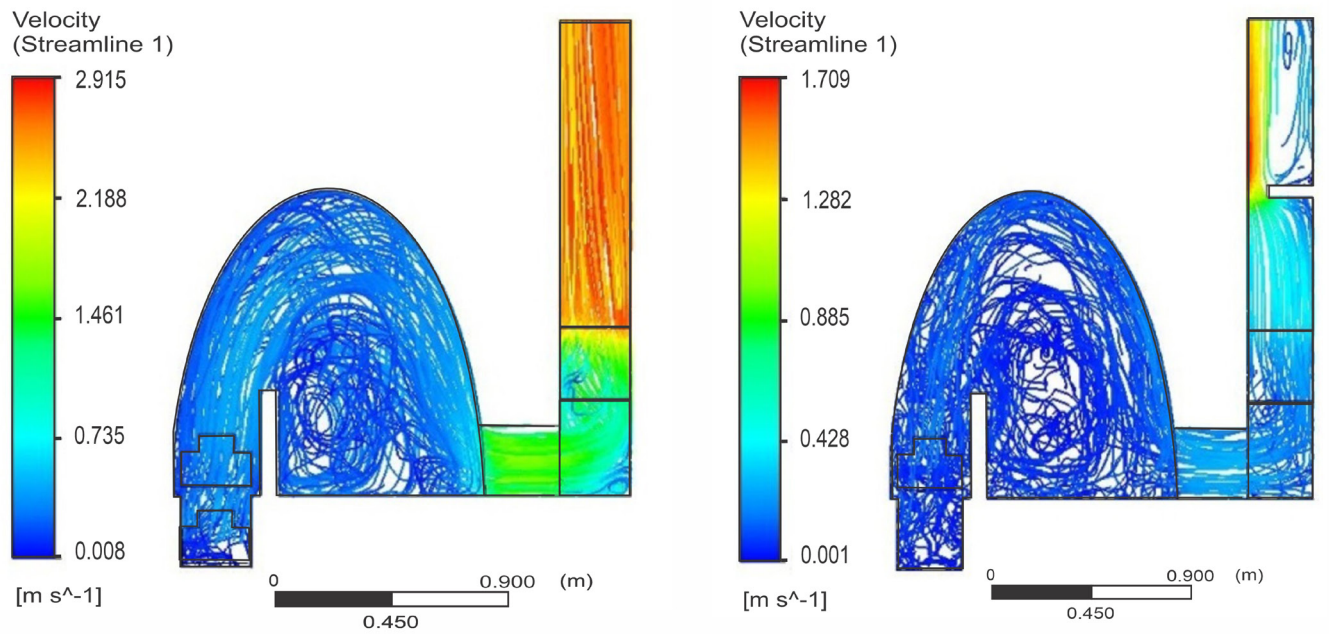

Figure 10: Current lines of velocity and turbulence occurring inside the domains studied in simulation B3, 100% open damper (a), and simulation B4, 50% open damper (b), of the family kiln.

levels were higher in the front region of the furnace, near the air inlet of the furnace and the chimney, after the damper, where the unburnt fuel in contact with the atmospheric air in this region recirculated. However, it was found that in this kiln the effect of the damper in the combustion process was contrary to that shown for the community kiln. In fact, the kiln with the totally opened damper produced a higher temperature field in the whole kiln. In the family kiln, the volumetric flow of butane was higher than that for the community kiln (Table III) and high air velocities could lead to better combustion, resulting in a smaller butane mass fraction inside the kiln, as can be observed in Figs. 9a and 9b, and to higher temperatures. The oxygen mass fractions are shown in Figs. 9c and 9d and the streamlines and velocity values are presented in Fig. 10. In simulation B3 there were regions with an excess of oxygen (Fig. 9c). These were regions where the flow had low speeds and low turbulence. In Fig. 10a this behavior at the top, near the catenary curve can be observed. Even if in this region the fuel mass fraction is very low, this oxygen concentration could help to burn the remaining fuel in the downstream regions and to produce higher kiln mean temperatures. In addition, the more intense air circulation in this case (Fig. 10a) could help to improve the heat convection across the kiln.

CONCLUSIONS

The new proposed kiln geometries improved the temperature levels and the energy efficiency of the firing. The simulations allowed a better understanding of the behavior of the most significant variables in the firing process of the studied ceramics. The simulations showed characteristics similar to those observed in experimental studies and in the literature. It was observed in simulation A that the velocity of the flue gases varied between 0.62 and 1.85 m/s, thus were coherent with the fourth principle of firing, where one notes that to ensure oxygenation of the average speed of furnace gases in the chimney should range between 1.2 to 1.5 m/s. The levels of temperature around 900 °C reached in simulations A (community kiln with open damper 100%/50%) and B (family kiln with open damper 100%/50%) were similar to those recorded with thermocouples at the end of the firings. It was noted that the frontal region appeared as the coldest region of the community and family furnaces both in the experiments and in the simulations. The four simulations showed consistent results, similar to the experimental ones, and showed how complex is the combustion process. The influence of boundary conditions on the results was identified through several preliminary simulations performed. The pressure in the air intake and in the chimney must be highlighted, because the increase in the back pressure caused by the damper closure must be reproduced, and consequently, reducing air circulation, besides the input speed of the fuel having been scaled by calculations. Comparing the productivity of the family and community kilns, the family kiln had a specific consumption of 4.7×10^{-3} kg/(m^3.s) while the community one presented 1.2×10^{-3} kg/(m^3.s), spending therefore 3.8 times more fuel per useful volume during the firing, and was, therefore, more interesting from the viewpoint of energy efficiency. The family kiln had higher levels of average temperatures during the firing procedure than the community oven, reaching 1300 ºC and offsetting its higher specific fuel consumption, and it may even improve if it burns at the highest temperatures reached. The two proposed kilns outperformed the temperature levels achieved by the local rudimentary kilns, which reached the maximum temperature level of 550 °C, indicating that the

improvements suggested are good alternatives to the firing process of the Jequitinhonha Valley community. The better performance of firing, geometry, and type of drawing of the two furnaces was explained by the promotion of the firing procedure and therefore reaching higher temperatures.

REFERENCES

[1] M. Fan, X. Zhou, S. Chen, S. Jiang, K. Gao, X. He, Silicon **30** (2022).
[2] Y. Tan, C. Li, Simulation **97** (2021) 311.
[3] P.C. Silva, L.P. Moreira, M.F.R.P. Alves, L.Q.B. Campos, B.G. Simba, C. dos Santos, Cerâmica **66**, 377 (2020) 30.
[4] C. Rohan, S. Jun, Surf. Coat. Technol. **385** (2020) 125324.
[5] C. Nolasco, G.G. Gómez Jácome, J.A. Gómez Campero, J. Phys. Conf. Ser. **1408** (2019) 12017.
[6] G. Guerrero Gómez, N. Afanador García, R.J. Gallardo Amaya, J. Phys. Conf. Ser. **2073** (2021) 12011.
[7] M. Żukowski, G. Woroniak, J. Piotrowska-Woroniak, Sol. Energy **194** (2019) 27.
[8] P. Punnarapong, T. Sucharitakul, N. Tippayawong, Energy Proc. **138** (2017) 622.
[9] M.N. Pedersen, M. Nielsen, C. Sønnik, J.P. Arendt, S.J. Lars, D.J. Kim, Energy Fuels **31** (2017) 11424.
[10] O.A. Kudryavtsev, S.B. Sapozhnikov, Int. J. Mech. Sci. **114** (2016) 60.
[11] M. Cargnin, S.M.A.G. Ulson Souza, A.A. Ulson Souza, A.J. Noni, Braz. J. Chem. Eng. **32** (2015) 433.
[12] S. Ferrer, A. Mezquita, V.M. Aguilella, E. Monfort, Appl. Therm. Eng. **150** (2015) 1002.
[13] S. Belz, Ceram. Tech. **34** (2012) 44.
[14] V.P. Nicolau, A.P. Dadam, J. Braz. Soc. Mech. Sci. Eng. **31**, 4 (2009) 297.
[15] J. Lawley, Ceram. Tech. **24** (2007) 36.
[16] T.S. Possamai, R. Oba, V.P. Nicolau, Appl. Therm. Eng. **48** (2012) 414.
[17] A.O. Nieckele, M.F. Naccache, M.S.P. Gomes, Appl. Therm. Eng. **31** (2011) 841.
[18] E. Hachem, G. Jannoun, J. Veysset, M. Henri, R. Pierrot, I. Poitrault, E. Massoni, T. Coupez, Simul. Model. Pract. Theory **30** (2013) 35.
[19] A. Abassi, K.H. Khoshmanesh, Appl. Therm. Eng. **28** (2008) 450.
[20] D.R. Dugwell, D.E. Oakley, Int. J. Heat Mass Transf. **31**, 11 (1988) 2381e90.
[21] S.A. Karaush, Y.I. Chizhik, E.G. Bober, Glass Ceram. **54**, 5 (1997) 190e2.
[22] R. Oba, T.S. Possamai, V.P. Nicolau, Appl. Therm. Eng. **63** (2014) 59.
[23] M.F. Naccache, M.S.P. Gomes, A.O. Nieckele, in Int. Heat Transfer Conf. **13** (2006).
[24] G.M. Santos, "Thermal behavior of a tunnel kiln applied in a structural ceramic industry", M.Sc. diss., UFSC, Florianópolis (2001).
[25] R.H. Essenhigh, Energy Fuels **15** (2001) 552.
[26] Z. Song, Fuel Energy Abstr. **39**, 3 (1998) 213.
[27] M.G. Carvalho, M. Nogueira, Appl. Therm. Eng. **17** (1997) 921.
[28] L. Zhao, G. Vahl Davis, E. Leonardi, in Int. Heat Transfer Conf., G.F. Hewitt (Ed.), **10** (1994) 183.
[29] J. Durakovic, S. Delalic, Mater. Geoenviron. **53**, 3 (2006) 403e8.
[30] E. Mancuhan, K. Kucukada, E. Alpman, J. Therm. Sci. Technol. **31**, 2 (2011) 79.
[31] H.A. Refaey, A. Abdel-Aziz Ali, R.K. Ali, H.E. Abdelrahman, M.R. Salem, Int. J. Therm. Sci. **122** (2017) 172.
[32] H.A. Refaey, A.A. Abdel-Aziz, M.R. Salem, H.E. Abdelrahman, M.W. Al-Dosoky, Int. J. Therm. Sci. **130** (2018) 264.
[33] CFX V11, "Reference guide", Ansys (2007).
[34] B.E. Launder, D.B. Spalding, Comput. Methods Appl. Mech. Eng. **3** (1974) 269.
[35] A.K. Colaciti, L.M.V. López, H.A. Navarro, L.C. Gómez, Appl. Math. Comput. **189**, 2 (2007) 1491.
[36] I. Gregory, *Kiln building*, A&C Black, London (1995).
[37] F.L. Olsen, *The kiln book: materials, specifications and constructions*, 2nd ed., A&C Black, London (1983).
[38] M.B. Cardoso, A.H. Ladio, S.M. Dutrus, M. Lozada, Biomass Bioenergy **81**, 7 (2015) 514.
[39] K. Kwiatkowski, E. Mastorakos, Energy Fuels **30**, 6 (2016) 4386.
[40] G. Nery, "Estudo do desempenho térmico de fornos catenários para queima de cerâmica artesanal", MSc diss., UFSJ, S. João Del Rei (2010).

(Rec. 22/06/2022, Rev. 11/07/2022, Ac. 20/07/2022)